Inorganic Chemistry

ARTICLE

pubs.acs.org/IC

Structure Resolution of $Ba_5Al_3F_{19}$ and Investigation of Fluorine Ion Dynamics by Synchrotron Powder Diffraction, Variable-Temperature Solid-State NMR, and Quantum Computations

Charlotte Martineau,*[,†] Franck Fayon,[‡,§] Matthew R. Suchomel,[⊥] Mathieu Allix,[‡,§] Dominique Massiot,[‡,§] and Francis Taulelle[†]

[†]Tectospin—Institut Lavoisier de Versailles, CNRS UMR 8180, Université de Versailles Saint-Quentin en Yvelines, 45 Avenue des États-Unis, 78035 Versailles Cedex, France

[‡]Conditions Extrêmes et Matériaux: Haute Température et Irradiation, CNRS UPR 3079, 1D Avenue de la Recherche Scientifique, 45071 Orléans Cedex 2, France

[§]Faculté des Sciences, Université d'Orléans, Avenue du Parc Floral, 45067 Orléans Cedex 2, France

[⊥]Advanced Photon Source, Argonne National Laboratory, Argonne, Illinois 60439, United States

Supporting Information

ABSTRACT: The room temperature structure of $Ba_5Al_3F_{19}$ has been solved using electron microscopy and synchrotron powder diffraction data. One-dimensional (1D) ^{27}Al and ultrafast magic-angle-spinning (MAS) ^{19}F NMR spectra have been recorded and are in agreement with the proposed structural model for $Ba_5Al_3F_{19}$. The ^{19}F isotropic chemical shift and ^{27}Al quadrupolar parameters have been calculated using the *CASTEP* code from the experimental and density functional theory geometry-optimized structures. After optimization, the calculated NMR parameters of both the ^{19}F and ^{27}Al nuclei show improved consistency with the experimental values, demonstrating that the geometry optimization step is necessary to obtain more accurate and reliable structural data. This also enables a complete and unambiguous assignment of the ^{19}F MAS NMR spectrum of $Ba_5Al_3F_{19}$. Variable-temperature 1D MAS ^{19}F NMR experiments have been carried out, showing the occurrence of fluorine ion mobility. Complementary insights were obtained from both two-dimensional (2D) exchange and 2D double-quantum dipolar recoupling NMR experiments, and a detailed analysis of the anionic motion in $Ba_5Al_3F_{19}$ is proposed, including the distinction between reorientational processes and chemical exchange involving bond breaking and re-formation.

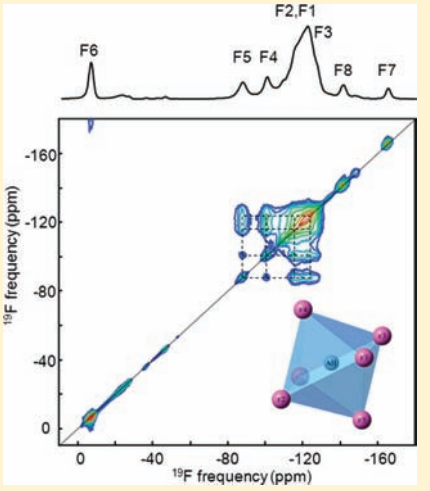

INTRODUCTION

BaF_2/AlF_3 is a rich chemical system containing numerous compounds:[1] trimorphic $BaAlF_5$, polymorphic Ba_3AlF_9, $Ba_3Al_2F_{12}$, $Ba_5Al_3F_{19}$, and Ba_5AlF_{13}. Two of these phases have similar stoechiometries: $B_3Al_2F_{12}$ (Ba/Al ratio of 1.5) and $Ba_5Al_3F_{19}$ (Ba/Al ratio of 1.67). $B_3Al_2F_{12}$ has been isolated, and its structure has been determined.[2,3] de Kozak et al. showed that, although $Ba_5Al_3F_{19}$ is more difficult to prepare, it can still be obtained by heating a stoichiometric mixture of 5:3 BaF_2/AlF_3 at 800 °C for a few hours.[1] Unit cell lattice parameters have been proposed (tetragonal symmetry, $a = 20.427$ Å, $c = 7.492$ Å, $Z = 8$, and P-type space group);[1] however, the crystal structure remains unresolved.

$Ba_5Al_3F_{19}$ is expected to adopt one of two structures commonly observed for purely fluorinated compounds belonging to the $Pb_5W_3O_9F_{10}$[4] family. These structures consist of a network of isolated and either edge-sharing octahedral-forming dimers ($Sr_5Fe_3F_{19}$,[5] $Sr_5Cr_3F_{19}$,[6] $Sr_5V_3F_{19}$,[6] and $Ba_5Fe_3F_{19}$[6]) or opposite corner-sharing $M^{III}F_6^{3-}$ (M^{III} = Al, Cr, Fe, Ga, Mn) octahedra forming infinite chains along the z direction ($Pb_5Cr_3F_{19}$,[7] phases II[8] and V[9] of $Pb_5Al_3F_{19}$, $Pb_5Ga_3F_{19}$,[10] $Ba_5Cr_3F_{19}$,[11] $Ba_5Mn_3F_{19}$,[6] and $Ba_5Ga_3F_{19}$[6]). In both cases, "free" F ions (not linked to any M^{III} cation) and the M^{II} cations (M^{II} = Ba, Pb, Sr) stand between octahedra. In these cited compounds, disorder on the fluorine position belonging to nonisolated $M^{III}F_6^{3-}$ octahedra and/or M^{II} cations is frequently observed. Although disorder of F ions can be difficult to probe by X-ray powder diffraction (XRPD), it can be conveniently described using high-resolution solid-state magic-angle-spinning (MAS) nuclear magnetic resonance (NMR).[10] The organization of the MF_6 polyhedra can also be responsible for the fluoride ion mobility, which can be followed by variable-temperature (VT) NMR exchange spectroscopy (EXSY), as reported for $Pb_5Ga_3F_{19}$.[12]

Received: December 20, 2010
Published: February 23, 2011

The present contribution deals with determination of the room temperature structure of $Ba_5Al_3F_{19}$ and investigation of the anionic mobility in this compound. Our strategy couples XRPD and transmission electronic microscopy (TEM) data with high-resolution solid-state NMR and density functional theory (DFT) calculations to refine the structure of $Ba_5Al_3F_{19}$ with a high accuracy, as was previously reported for other inorganic fluorides.[10,13,14] Diffraction data are obtained from both laboratory and synchrotron X-ray sources. One-dimensional (1D) ^{27}Al and ultrafast MAS ^{19}F NMR experiments allow probing of the number of distinct F and Al crystallographic sites and their multiplicities. After a structure optimization step, the ^{19}F chemical shift and ^{27}Al electric field gradient (EFG) tensors are calculated using the DFT *CASTEP* code.[15,16] This affords an unambiguous assignment of the ^{19}F NMR spectrum. Moreover, the good agreement between the calculated and experimental ^{27}Al quadrupolar coupling constants attests to the accuracy of the optimized structure of $Ba_5Al_3F_{19}$. Finally, ^{19}F MAS VT and 2D EXSY and double-quantum single-quantum (DQ−SQ) NMR experiments are employed to characterize the fluoride ion mobility in $Ba_5Al_3F_{19}$, and a model of the fluoride mobility is proposed.

MATERIALS AND METHODS

1. Synthesis. As was reported previously,[1] $Ba_5Al_3F_{19}$ was prepared by heating a stoichiometric mixture of 5:3 BaF_2/AlF_3 at 800 °C for a few hours. Inspection of the XRPD data shows, in addition to the majority phase $Ba_5Al_3F_{19}$, the presence of $Ba_3Al_2F_{12}$ as a minor impurity.

2. Diffraction. A room temperature XRPD diffractogram of $Ba_5Al_3F_{19}$ was collected overnight on a Siemens D5000 diffractometer using a monochromated Cu Kα radiation (λ = 1.5406 Å) in the 10−160° 2θ range with an interpolated step of 0.01°. High-resolution synchrotron powder diffraction (SPD) data have been recorded on the 11-BM diffractometer at the Advanced Photon Source, Argonne National Laboratory. Data were collected over the 0.5−50° 2θ range with a 0.001° step size at room temperature using a wavelength of λ = 0.412 213 Å. The sample was contained in a 0.5 mm glass capillary and was spun at 60 Hz during data collection. The Rietveld[17] method implemented in the *Fullprof*[18] program was used for the structure refinement of $Ba_5Al_3F_{19}$.

3. TEM. The sample for TEM was prepared by crushing the powder of $Ba_5Al_3F_{19}$ in *n*-butanol, and the small crystallites in suspension were deposited onto a holey carbon film, supported by a copper grid. The electron diffraction (ED) study was carried out with a Philips CM20 transmission electron microscope. Energy-dispersive spectroscopy (EDS) analyses were systematically carried out during the ED study, with the CM20 microscope being equipped with an Oxford EDAX analyzer. Although fluoride materials are not usually studied by TEM because they tend to quickly become amorphous under the beam, we were able to study the $Ba_5Al_3F_{19}$ compound by carefully spreading out the beam.

4. NMR Spectroscopy. The one-pulse MAS (25 kHz) ^{27}Al (nuclear spin $I = {}^5/_2$) NMR spectrum of $Ba_5Al_3F_{19}$ was recorded at T = 45 °C on an Avance 500 Bruker spectrometer (B_0 = 11.6 T, ^{27}Al Larmor frequency of 130.3 MHz) using a 2.5 mm MAS probe. A pulse duration of 1 μs (11° tip angle) was employed with a recycle delay of 1 s, and 21 000 transients were accumulated.

The VT (28−90.5 °C temperature range) MAS (54 kHz) Hahn-echo ^{19}F NMR spectra were recorded on an Avance 300 Bruker spectrometer (B_0 = 7.0 T; ^{19}F Larmor frequency 282.2 MHz) using an ultrafast MAS 1.3 mm probe. The 90° pulse length was 1.1 μs (corresponding to a nutation frequency of ∼225 kHz), and the recycle delay was set to 10 s. The sample temperature was calibrated using the ^{207}Pb isotropic chemical shift of $Pb(NO_3)_2$ as the NMR thermometer[19,20] and was monitored using a Bruker VT unit.

2D EXSY MAS[21] ^{19}F NMR spectra were acquired at B_0 = 7.0 T using an ultrafast spinning rate (54 kHz), allowing rotor synchronization of the t_1 increment to avoid the presence of a spinning sideband in the indirect dimension. The EXSY spectra were recorded with a mixing time of 2 ms. A total of 220 rotor-synchronized t_1 increments with 16 transients each were accumulated, and phase-sensitive detection in the indirect dimension was achieved using the States method.[22]

2D homonuclear DQ−SQ MAS (54 kHz) ^{19}F NMR correlation spectra were collected at B_0 = 7 T using the sandwiched PI pulses (SPIP)[23] pulse sequence, which allows efficient broad-band homonuclear DQ recoupling in inorganic fluorides.[24,25] ^{19}F nutation frequencies of 225 kHz for the π pulse and of 80 kHz for the spin lock were used, and the DQ excitation and reconversion times were set to 12 rotor periods (corresponding to ∼220 μs). A total of 78 rotor-synchronized t_1 increments with 32 transients each were accumulated. Phase-sensitive detection in the indirect dimension was obtained using the States method.[22] The 2D DQ−SQ MAS spectra were converted in a SQ−SQ correlation representation by a shearing transformation.[26,27]

The SPIP and EXSY spectra were both recorded at T = 28 and 90 °C. The ^{19}F and ^{27}Al chemical shifts were referenced to $CFCl_3$ and a 1 M $Al(NO_3)_3$ solution, respectively. NMR spectra were reconstructed using the *DMFit*[28] software.

5. Ab Initio Calculations. Calculations of the NMR parameters were performed with the *CASTEP*[15,16] DFT code in the Materials Studio 5.0 environment using projector-augmented waves (PAW)[29] and gauge-included PAW (GIPAW)[30] algorithms for the EFGs and NMR chemical shifts, respectively. The Perdew−Burke−Ernzerhof (PBE) functional[31] was used in the generalized gradient approximation (GGA) for the exchange-correlation energy, and the core−valence interactions were described by ultrasoft pseudopotentials.[32] For ^{19}F, a core radius of 1.4 Å was used with 2s and 2p valence orbitals, for ^{27}Al, a core radius of 2.0 Å was used with 3s and 3p valence orbitals, and for ^{137}Ba, a core radius of 2.9 Å was used with 5s, 5p, and 6s valence orbitals. The wave functions were expanded on a plane-wave basis set with a kinetic energy cutoff of 600 eV. The Brillouin zone was sampled using a Monkhorst−Pack grid spacing of 0.04 Å^{-1}. Computations of the NMR parameters were performed for both the experimental and geometry-optimized structures of $Ba_3Al_5F_{19}$. The Broyden−Fletcher−Goldfarb−Shanno (BFGS) minimization method was used for structure optimization,[33] and the cell parameters were set to those determined by XRPD and kept constant. After geometry optimization, forces were lower than 8 meV Å^{-1} for all atoms.

RESULTS AND DISCUSSION

1. Room Temperature Structure. *1.1. Structure Refinement.* As mentioned earlier, although no structural model has been proposed to date, de Kozak et al. have reported preliminary cell parameters for $Ba_5Al_3F_{19}$: a = 20.427 Å, c = 7.492 Å, with Z = 8 and a primitive lattice.[1] However, we find that a smaller quadratic unit cell ($a \sim$ 14.57 Å and $c \sim$ 7.46 Å) with space group $I4/m$ (No. 87) and Z = 4, i.e., the same unit cell as that of the related compounds $Sr_5M_3F_{19}$ (M = Cr, Fe, V), $Ba_5Ga_3F_{19}$, and $Pb_5Al_3F_{19}$-II, allows indexing of all observed diffraction peaks in both the XRPD and SPD data sets for $Ba_5Al_3F_{19}$. The ED study (Figure 1) confirmed the quadratic cell and the absence of any observed special condition coupled to the general reflection condition hkl, $h + k + l = 2n$, which indicates an I lattice with eight possible space groups: $I4$, $I\bar{4}$, $I4/m$, $I422$, $I4mm$, $I\bar{4}2m$, $I4/mmm$, and $I\bar{4}m2$. Therefore, the quadratic cell ($a \approx$ 14.5 Å and

dx.doi.org/10.1021/ic102534d |*Inorg. Chem.* 2011, 50, 2644–2653

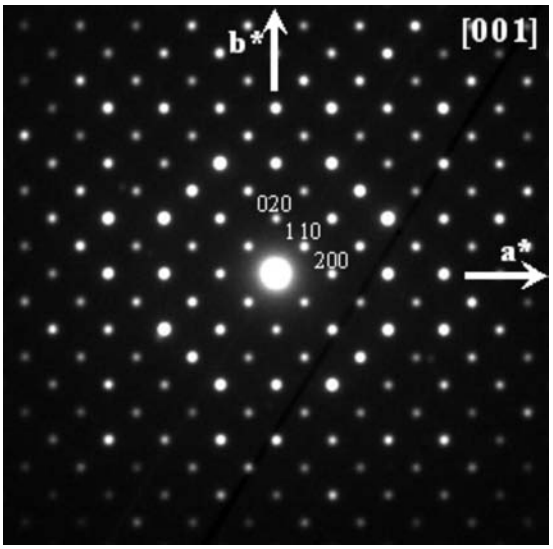

Figure 1. Experimental [001] ED pattern of $Ba_5Al_3F_{19}$.

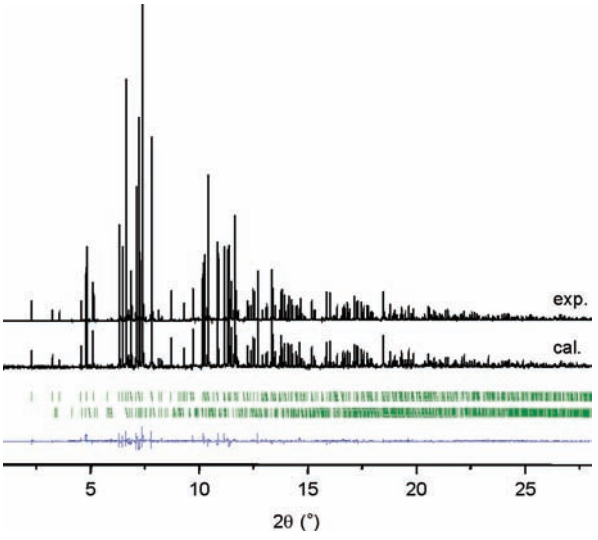

Figure 2. Experimental and calculated room temperature SPD patterns of $Ba_5Al_3F_{19}$. The Bragg positions (vertical ticks) and the differences between the experimental and calculated data (in blue) are shown. The fit statistics are R_p = 7.4%, R_{wp} = 10.6%, and R_{Bragg} = 4.1%.

$c \approx 7.5$ Å) with the $I4/m$ space group was chosen. EDS analyses have been carried out on the studied crystallites and confirmed a Ba/Al cation ratio of 5:3.

The cell parameters were refined by whole-pattern matching of the XRPD diagram to the following values: a = 14.576(1) Å and c = 7.460(1) Å. In order to perform a Rietveld refinement of the SPD diagram, the atomic coordinates of the isostructural $Pb_5Al_3F_{19}$-II[8] were used as starting data (Ba atoms replacing Pb atoms). $Ba_3Al_2F_{12}$, whose structure is known,[2,3] is present as an impurity (~8% mol) in the sample and was included in the refinement. After several refinement iterations, satisfactory fit statistics were obtained: R_p = 7.4%, R_{wp} = 10.6%, and R_{Bragg} = 4.1% (Figure 2). Atomic parameters of $Ba_5Al_3F_{19}$ are gathered in Table 1.

The structure of $Ba_5Al_3F_{19}$ (Figure 3) contains two 6-fold-coordinated Al, three Ba, and eight crystallographically

Table 1. Atom Label, Wyckoff Multiplicity, Site Symmetry, Atomic Positions *x*, *y*, and *z* Deduced from the Rietveld Refinement,[a] Atomic Positions *x*, *y*, *z* (in Italics) of the Geometry-Optimized Structure of $Ba_5Al_3F_{19}$, and Isotropic Displacement Parameter B_{iso} (Å^2)[b]

atom	Wyckoff	site symmetry	*x*	*y*	*z*	B_{iso}
Ba1	8h	*m*..	0.08485(4)	−0.24030(4)	0	0.78(1)
			0.0864	*−0.2398*	*0*	
Ba2	8h	*m*..	−0.05750(5)	−0.21398(4)	$^1/_2$	1.20(1)
			−0.0538	*−0.2133*	$^1/_2$	
Ba3	4d	$\bar{4}$..	0	$^1/_2$	$^1/_4$	1.21(1)
			0	$^1/_2$	$^1/_4$	
Al1	8h	*m*..	0.1606(3)	0.3208(2)	0	0.73(5)
			0.1583	*0.32195*	*0*	
Al2	4e	4..	0	0	0.2435(9)	1.09(8)
			0	*0*	*0.2464*	
F1	16i	1	0.3894(2)	0.4497(3)	0.2383(5)	1.74(1)
			0.3885	*0.4496*	*0.2414*	
F2	16i	1	0.1984(2)	0.4076(3)	0.1679(5)	1.56(2)
			0.1962	*0.4047*	*0.1693*	
F3	16i	1	0.3882(3)	0.2528(3)	0.6602(5)	2.4(1)
			0.3858	*0.2577*	*0.6667*	
F4	8h	*m*..	0.2610(5)	0.2650(4)	0	2.9(1)
			0.2676	*0.2656*	*0*	
F5	8h	*m*..	0.4471(4)	0.1201(4)	$^1/_2$	1.8(1)
			0.4526	*0.1238*	$^1/_2$	
F6	8h	*m*..	0.4203(4)	0.1180(3)	0	0.6(2)
			0.4250	*0.1165*	*0*	
F7	2a	4/*m*..	0	0	0	2.4(2)
			0	*0*	*0*	
F8	2b	4/*m*..	0	0	$^1/_2$	2.4(2)
			0	*0*	$^1/_2$	

[a] Refined cell parameters: a = 14.576 Å; c = 7.460 Å. [b] Uncertainties on the experimental atomic positions are given in brackets.

inequivalent F atoms (Table 1), arranged in a network of isolated $Al1F_6^{3-}$ octahedra and infinite chains of $Al2F_6^{3-}$ octahedra running along the c crystallographic axis. Between these are located the Ba atoms and F6 "free" F atoms, which do not belong to any AlF_6^{3-} octahedron. There are two bridging F atoms, F7 and F8, linking two $Al2F_6^{3-}$ octahedra and five nonbridging F atoms, F1, F2, F3, F4, and F5, belonging to the AlF_6^{3-} octahedra (F1 from the $Al2F_6^{3-}$ octahedron and F2, F3, F4, and F5 from the isolated $Al1F_6^{3-}$ octahedron). Although most of the compounds from the family $M^{II}M^{III}F_{19}$ (M^{II} = Ba, Pb, Sr; M^{III} = Al, Cr, Fe, Ga, Mn) show a static disorder on either M^{II} or nonbridging F sites, a satisfactory Rietveld refinement is obtained for $Ba_5Al_3F_{19}$ using an ordered structural model (Figure 2).

1.2. NMR Experiments

Solid-State ^{27}Al NMR. The MAS ^{27}Al NMR spectrum of $Ba_5Al_3F_{19}$ recorded at T = 45 °C with a spinning frequency of 25 kHz is shown in Figure 4. Under this MAS frequency, ^{19}F decoupling has no influence on the ^{27}Al NMR spectrum and does not enhance the spectral resolution. This MAS spectrum exhibits two lines with relative intensities of 32% and 68% (Figure 4) assigned to Al2 (Wyckoff multiplicity 4 of site-point symmetry 4..) and Al1 (Wyckoff multiplicity 8 of site-point symmetry *m*..), respectively. The ^{27}Al isotropic chemical shifts

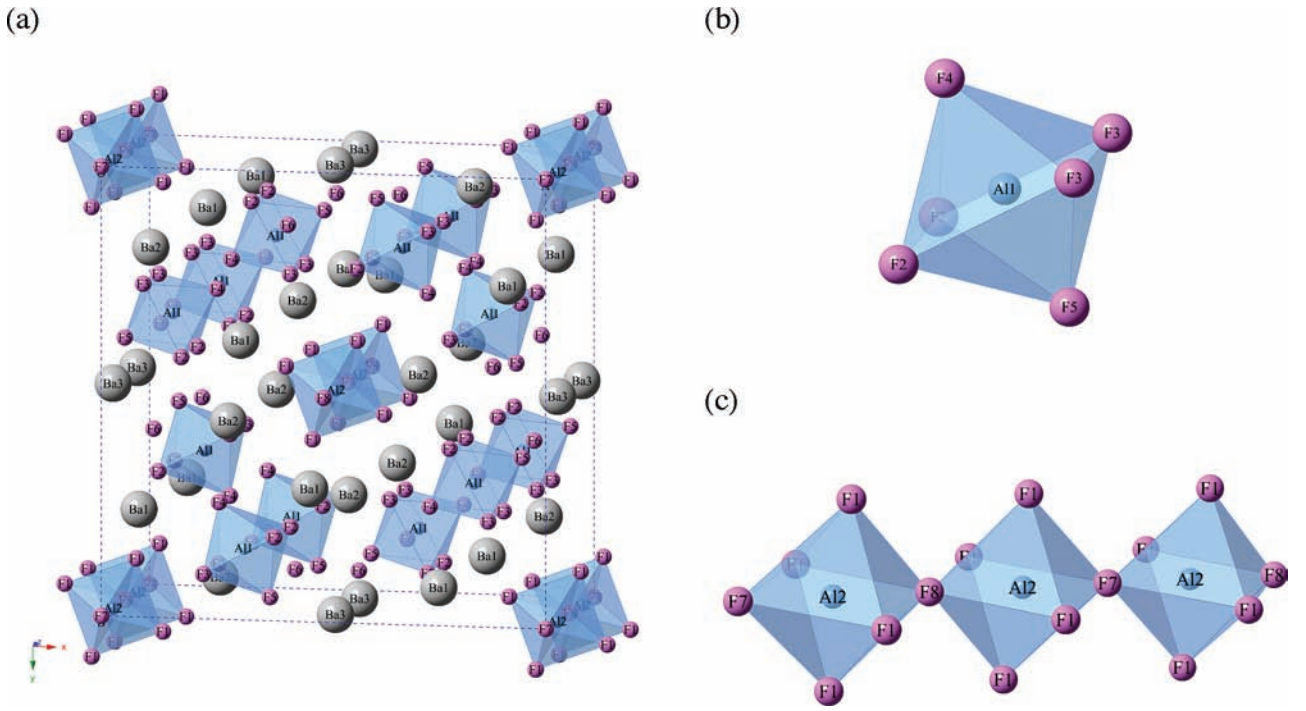

Figure 3. (a) Perspective view of the structure of $Ba_5Al_3F_{19}$. Representation of the (b) isolated $Al1F_6^{3-}$ and (c) chains of $Al2F_6^{3-}$ octahedra on which the atoms are labeled.

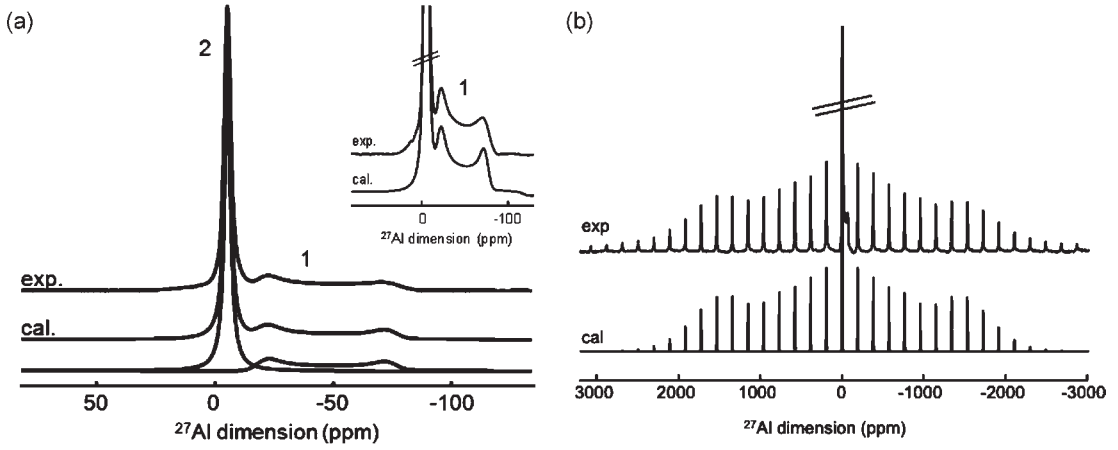

Figure 4. Experimental and reconstructed central transition (a) and spinning sideband manifold of line 2 (b) of the MAS ^{27}Al NMR (25 kHz) spectrum of $Ba_5Al_3F_{19}$ recorded at 11.6 T. An expansion of line 1 is presented in the inset.

(δ_{iso}) of these two resonances are typical of octahedral AlF_6 sites. The quadrupolar parameters of Al2 were determined from reconstruction of the central transition (Figure 4a), while the quadrupolar parameters of Al1, whose central transition is shapeless (Figure 4a), were determined from reconstruction of the satellite transition spinning sideband manifold (Figure 4b). A well-defined set of parameters (Table 2) is used for reconstruction of the NMR spectrum, indicating that the AlF_6^{3-} octahedra are rigid and that there is no static disorder in the polyhedra, i.e., no distribution of F sites. The Al1 resonance has a small quadrupolar coupling constant (C_Q) of 1.9 MHz, characteristic of isolated AlF_6^{3-} octahedra.[34] The Al2 resonance exhibits a much larger C_Q value of 11.3 MHz, as expected for an Al atom in an AlF_6^{3-} octahedron that contains both nonbridging and bridging F ions.[35,36] Al2 has an asymmetry parameter $\eta_Q = 0$ characteristic of an axially symmetric quadrupolar coupling tensor, in agreement with its location in a special position with 4-fold axis symmetry (Table 1).

Solid-State ^{19}F NMR. The room temperature (T = 28 °C) Hahn-echo ^{19}F NMR spectrum of $Ba_5Al_3F_{19}$ recorded at ultrafast MAS (54 kHz) and moderate magnetic field (7 T) is shown in Figure 5. In addition to the intense ^{19}F resonances of $Ba_5Al_3F_{19}$, this spectrum also shows minor peaks belonging to $Ba_3Al_2F_{12}$, known to be present as an impurity in the sample. Eight ^{19}F lines are used to reconstruct the MAS ^{19}F NMR spectrum (Table 3) of $Ba_5Al_3F_{19}$, as expected from the structure. The NMR spectrum therefore confirms the absence of distribution of F sites and also indicates the absence of distribution of the Ba sites in $Ba_5Al_3F_{19}$ (which would have generated additional F resonances). According to their relative intensities, resonances 1 and 2 (of relative

dx.doi.org/10.1021/ic102534d |*Inorg. Chem.* 2011, 50, 2644–2653

Table 2. Experimental ^{27}Al Isotropic Chemical Shift (δ_{iso}), Quadrupolar Coupling Constant (C_Q), and Asymmetry Parameter (η_Q) Determined from Reconstruction of the ^{27}Al NMR Powder Spectrum of $Ba_5Al_3F_{19}$ and DFT-Calculated NMR Parameters for Both the SPD and DFT Geometry-Optimized Structures of $Ba_5Al_3F_{19}$[a]

	experimental			calculated SPD structure			calculated geometry-optimized structure		
site	δ_{iso} (ppm)	C_Q (MHz)	η_Q	δ_{iso}[b] (ppm)	C_Q[c] (MHz)	η_Q	δ_{iso}[b] (ppm)	C_Q[c] (MHz)	η_Q
Al1	−2.5(0.5)	1.9(1)	0.8(1)	4.6	−7.42	0.44	−1.8	2.30	0.79
Al2	−1.0(0.5)	11.3(1)	0.0(1)	−0.5	11.21	0	−2.4	10.69	0

[a] The ^{27}Al NMR powder spectrum of $Ba_5Al_3F_{19}$ is not sensitive to the sign of C_Q, and only the absolute values of the calculated C_Q's are to be compared to the experimental ones. [b] With $\delta_{iso} = 541.2 - \sigma_{iso}$. [c] Using the quadrupolar moment value of 1.466 10^{-29} m^2 reported by Pyykkö (Pyykkö, P. *Mol. Phys.* **2001**, *99*, 1617−1629; **2008**, *106*, 1965−1974).

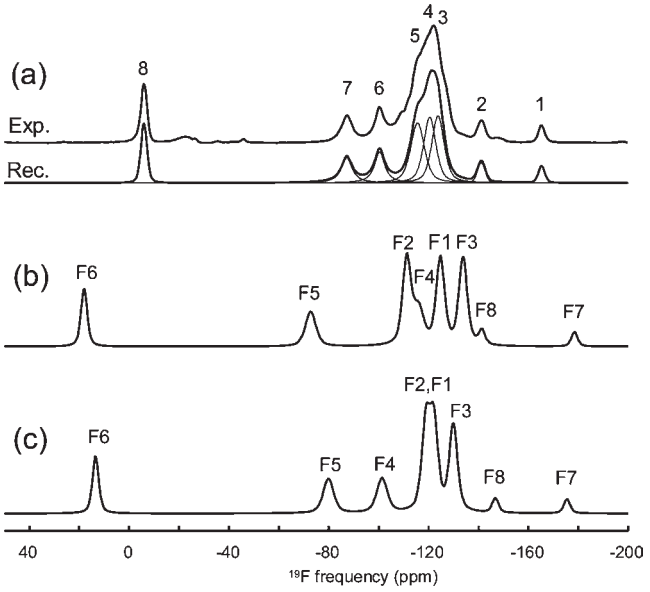

Figure 5. (a) Experimental and reconstructed MAS ^{19}F NMR (54 kHz) spectra of $Ba_5Al_3F_{19}$ recorded at B_0 = 7 T and T = 28 °C. Individual contributions are shown. Unlabeled peaks belong to $Ba_3Al_2F_{12}$. GIPAW DFT-calculated ^{19}F NMR spectra for the SPD (b) and geometry-optimized (c) structures of $Ba_5Al_3F_{19}$. In parts b and c, the linewidths of the resonances were arbitrarily chosen and the integrated intensities correspond to the site multiplicities. The calculated spectra were referenced such that their barycenters correspond to the barycenter of the experimental spectrum.

intensity ∼3%) correspond to the bridging F ions F7 and F8 (Wyckoff multiplicity 2), lines 6−8 (of relative intensity ∼10%) correspond to F4, F5, and F6 (Wyckoff multiplicity 8), and lines 3−5 (of relative intensity ∼21%) are assigned to F1, F2, and F3 (Wyckoff multiplicity 16). This assignment is consistent with the known ^{19}F isotropic chemical shift (δ_{iso}) range in inorganic barium aluminofluorides:[37] the bridging F atoms have the lowest isotropic chemical shifts, the free F atoms have the highest isotropic chemical shifts, and in between stands the isotropic chemical shift range for the nonbridging F atoms. For each of these types of F atoms (i.e., bridging, nonbridging, or free), it has been shown that the ^{19}F isotropic chemical shift depends on the number of first Ba neighbors and their distance to the F atoms (providing similar Al−F and F−F distances): a larger number of Ba neighbors and shorter Ba−F interatomic distances give rise to a higher ^{19}F isotropic chemical shift.[38] Following this empirical correlation, line 8, with the highest δ_{iso} (−6 ppm), is assigned to the "free" F ion F6 (consistent with its relative intensity) and lines1 and 2 (at −164 and −140 ppm) are assigned respectively

Table 3. Line Label, ^{19}F Experimental Isotropic Chemical Shift (δ_{iso}^{exp}), Relative Intensity (I), and Calculated Isotropic Chemical Shifts (δ_{iso}^{calc}) for the SPD and Geometry-Optimized Structure and Proposed Line Assignment

					δ_{iso}^{calc}(ppm)	
line	δ_{iso}^{exp} (ppm)	I (%)	site	multiplicity	SPD[a]	geometry optimized[a]
1	−164	3(1)	F7	2	−178.5	−175.5
2	−140	3(1)	F8	2	−141.4	−146.8
3	−125	22(1)	F3	16	−133.9	−130.0
4	−120	22(1)	F1	16	−124.8	−122.2
5	−116	22(1)	F2	16	−111.3	−119.0
6	−100	10(1)	F4	8	−116.0	−101.4
7	−87	9(1)	F5	8	−72.8	−79.9
8	−6	9(1)	F6	8	18.0	13.4

[a] Using an arbitrary chemical shift reference that makes the barycenters of the calculated and experimental ^{19}F NMR spectra coincident.

to the bridging F atoms F7 and F8 because F7 has four Ba neighbors at 3.715 Å and F8 has four Ba neighbors at a shorter distance of 3.207 Å (see Table S1 in the Supporting Information, SI). Similarly, resonances 6 and 7 (with relative intensity 10.5%) can be assigned to the nonbridging F4 and F5 atoms, which have two and three Ba neighbors at a similar distance of ∼2.6 Å, respectively. However, this empirical relationship does not allow a detailed assignment of the three remaining resonances (lines 3−5) to the nonbridging F1, F2, and F3 atoms having a very similar environment. To go further in the attribution of the ^{19}F resonances to the crystallographic F sites of the $Ba_5Al_3F_{19}$ structure, we have performed DFT calculations of the ^{19}F isotropic chemical shifts on the basis of a periodic structure model, which was shown to reproduce with a very good accuracy the ^{19}F experimental chemical shift of various inorganic metal fluorides.[39]

1.3. DFT Calculations of the NMR Parameters: Optimization and Validation of the Structural Model. The DFT calculations of the NMR parameters for $Ba_5Al_3F_{19}$ have been carried out using the NMR *CASTEP* package.[15,16] Because $Ba_5Al_3F_{19}$ contains both heavy (Ba) and light (F) atoms, a precise location of the F atoms in the unit cell from SPD data remains difficult. Therefore, NMR parameter calculations were performed for both the experimental SPD and DFT geometry-optimized structures. For the geometry optimization step, atomic coordinates were allowed to vary while the unit cell parameters were kept fixed to the values determined by X-ray diffraction. The average quadratic atomic displacements resulting from geometry optimization range from 0.022 to 0.097 Å, with the largest ones being those of F atoms F3, F4, F5, and F6 (Figure 6a). This leads

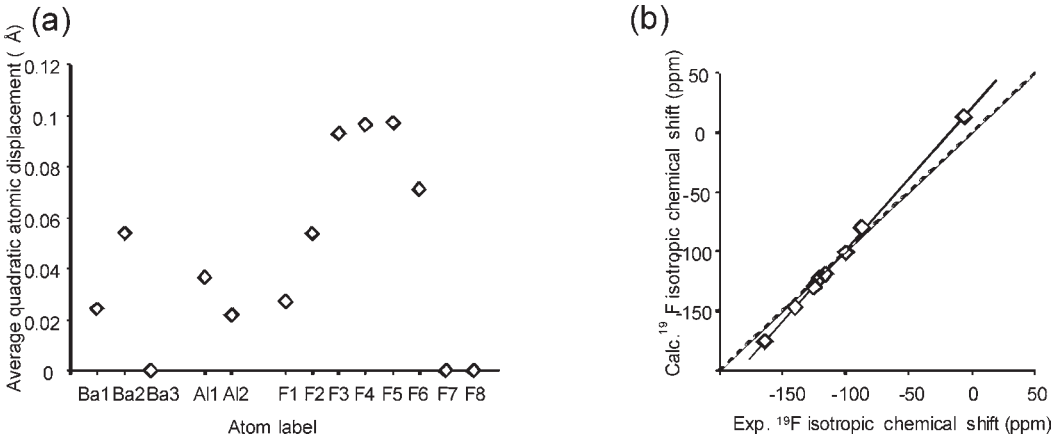

Figure 6. (a) Average quadratic atomic displacement resulting from geometry optimization (DFT GGA−PBE) of the $Ba_5Al_3F_{19}$ structure. (b) Experimental vs calculated (geometry-optimized structure) ^{19}F isotropic chemical shifts in $Ba_5Al_3F_{19}$. The calculated isotropic chemical shifts were arbitrarily referenced such that the barycenters of the calculated and experimental spectra were coincident. The solid line represents a linear fit ($\delta_{iso}^{exp} = -0.83\delta_{iso}^{cal} - 17.6$, with $R^2 = 0.999$). The dashed line indicates a diagonal with a slope of 1.

to a shortening of the average Ba−F bond lengths of about 0.01 Å and to an increase of the Al−F average bond lengths (of 0.03 Å for Al1 and of 0.01 Å for Al2), associated with a decrease of both Ba−F and Al−F bond length variances and to a decrease of the distortions of the AlF_6 octahedral units (longitudinal strains[40] decrease from 0.19 to 0.05 for the $Al1F_6$ octahedron and from 0.13 to 0.11 for the $Al2F_6$ octahedron; shear strains[40] decrease from 0.84 to 0.45 for the $Al1F_6$ octahedron and from 0.64 to 0.42 for the $Al2F_6$ octahedron). The geometry-optimized structure (GGA approximation with a PBE functional) also leads to an acceptable match of the experimental SPD with reliability factor $R_p = 9.2\%$, $R_{wp} = 11.6\%$, $R_{Bragg} = 5.8\%$ (see Figure S3 in the SI).

The results of GIPAW DFT calculations of the ^{19}F and ^{27}Al isotropic chemical shifts and ^{27}Al quadrupolar coupling parameters for the $Ba_5Al_3F_{19}$ SPD and geometry-optimized structures are given in Tables 2 and 3. As shown in Figure 5b, there is a discrepancy between the experimental ^{19}F NMR spectrum and the spectrum calculated for the SPD structure, with the calculated isotropic chemical shift of the F4 site with multiplicity 8 being incorrect relative to that of F sites with multiplicities of 16. This discrepancy is solved for the ^{19}F spectrum calculated after geometry optimization (Figure 5c), thereby allowing assignment of the ^{19}F resonances of the $Ba_5Al_3F_{19}$ MAS NMR spectrum (see Table 3). It should be noted that the initial partial assignment proposed on the basis of empirical arguments (number and distance of the first Ba neighbors) is in agreement with this final assignment obtained from GIPAW DFT calculation of the ^{19}F chemical shifts for the geometry-optimized $Ba_3Al_5F_{19}$ structure. Figure 6b shows a comparison between experimental and calculated (after geometry optimization of the structure) ^{19}F isotropic chemical shifts. A good linear correlation is observed with a relationship ($\delta_{iso}^{exp} = -0.83\ \delta_{iso}^{cal} - 17.6$, with $R^2 = 0.999$) very close to the one reported for single-F-site inorganic fluoride compounds.[39] As for the ^{19}F isotropic chemical shifts, there are significant discrepancies between the experimental ^{27}Al NMR parameters (^{27}Al isotropic chemical shifts and quadrupolar parameters of the Al1 site) and those calculated for the SPD structure, again confirming inaccurate locations of some atoms in the SPD structure. The agreement between the ^{27}Al NMR parameters calculated for the optimized structure and the experimental values is much better, in particular for the quadrupolar coupling constant C_Q and asymmetry parameter η_Q of Al1 (Table 2), indicating that the AlF_6^{3-} octahedral units are more accurately described in the geometry-optimized structure. In conclusion, the DFT geometry-optimized structure, being validated by two distinct sets of experimental NMR parameters (^{19}F and ^{27}Al), appears to be more reliable than that directly obtained from Rietveld refinement of the experimental SPD diagram.

2. Fluoride Ion Mobility. In $Pb_5Ga_3F_{19}$, whose structure is closely related to that of $Ba_5Al_3F_{19}$, we have recently evidenced a mutual chemical exchange above 30 °C between all of the F sites of the isolated octahedral units of the structure.[12] Therefore, we have investigated the possible occurrence of a similar dynamical process in $Ba_5Al_3F_{19}$ using VT MAS and 2D EXSY ^{19}F NMR experiments.

As shown in Figure 7, the VT MAS ^{19}F NMR (54 kHz) spectra of $Ba_5Al_3F_{19}$ recorded between 28 and 64 °C show a broadening with an increase in the temperature of the ^{19}F resonances corresponding to the F ions F2, F3, F4, and F5. For a temperature higher than 70 °C, these resonances coalesce into a single line (labeled B) located at − 111 ppm, which is the weighted average of the isotropic chemical shifts at room temperature of the coalescing peaks (Table 3). This observation is an indication of a correlated motion of these F ions, located at the six corners of the isolated $Al1F_6^{3-}$ octahedral units. Coalescence is reached at $T \sim 72$ °C, and at this temperature, the correlation time τ_c of the motion is 41×10^{-5} s ($\tau_c = \pi\sqrt{2}/\Delta\nu$, where $\Delta\nu = 10.7$ kHz is the maximum chemical shift difference between the F sites involved in the exchange process). For higher temperature, the increase of the motion rate results in a narrowing of line B. One should notice that the intensity of line B is less than the sum of the line intensity of F2, F3, F4, and F5, indicating that the fast regime of motion is not reached yet, even at the maximum temperature investigated ($T = 93$ °C). The MAS ^{19}F NMR spectra recorded upon cooling (not shown) were identical with the spectra recorded during heating, indicating that the process is reversible without hysteresis. The chemical shifts, linewidths, and relative intensities of the lines assigned to the F ions F1, F7, and F8 belonging to the $Al2F_6^{3-}$ octahedra do not evolve significantly with the temperature, indicating that they are not involved in a dynamic process with a time scale smaller than 36×10^{-5} s,

dx.doi.org/10.1021/ic102534d |Inorg. Chem. 2011, 50, 2644–2653

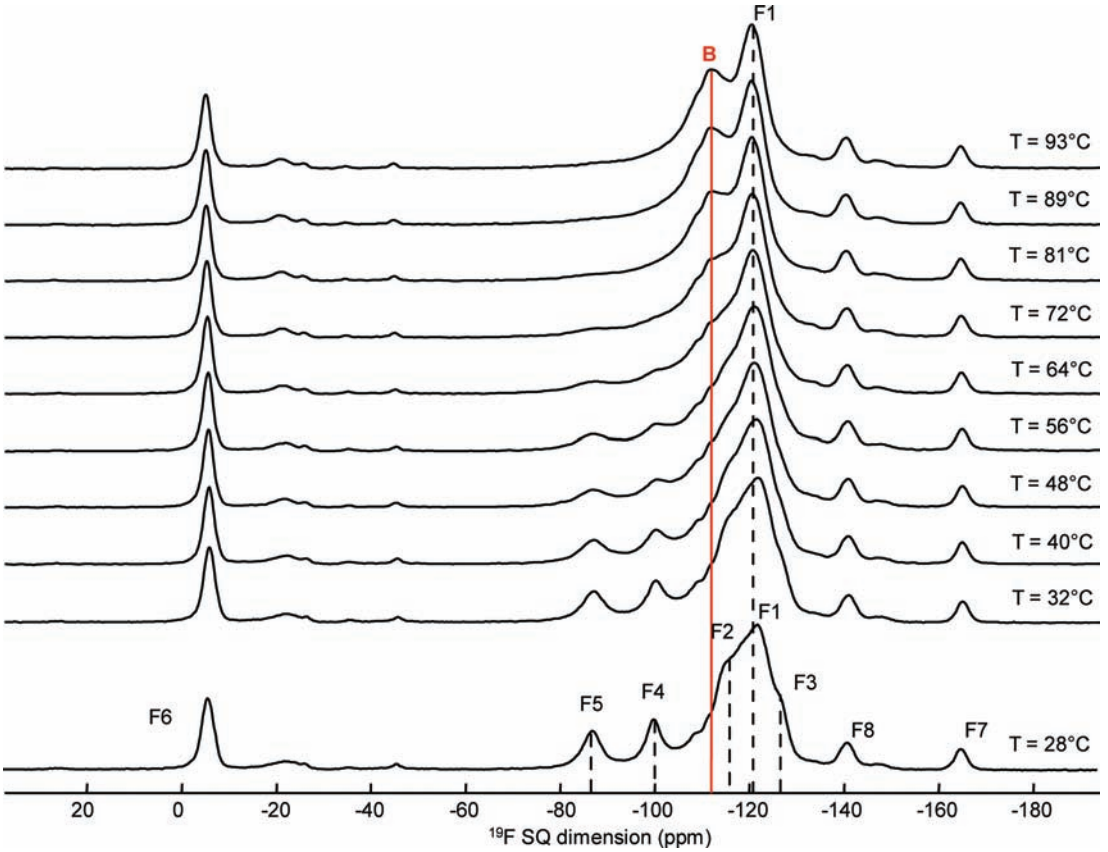

Figure 7. VT MAS Hahn−echo ^{19}F NMR (54 kHz) spectra of $Ba_5Al_3F_{19}$ recorded at 7 T. Dashed lines indicate the position of the nonbridging F ions F2, F3, F4, and F5 at 28 °C. The narrow line indicates the position of the nonbridging F1 ion and the thick line the position of the line labeled B. Small unlabeled peaks belong to $Ba_3Al_2F_{12}$.

at least, for temperatures below 90 °C. It should be noted that a possible motion of the free F6 ions consisting of jumps between equivalent crystallographic sites cannot be evidenced from these 1D MAS experiments and is therefore not excluded.

To obtain further information on the fluorine dynamical process, 2D EXSY MAS ^{19}F NMR experiments[21] were carried out at different temperatures. In this experiment, chemical exchange occurring on the time scale of the mixing time is revealed by off-diagonal cross-correlation peaks between distinct resonances. To avoid the presence of a cross-correlation peak due to a ^{19}F spin diffusion process (i.e., a magnetization transfer through homonuclear ^{19}F dipolar couplings)[34,41−43] in EXSY MAS spectra, ultrafast MAS (54 kHz) and a short mixing time (2 ms) were employed.[44] The 2D EXSY ^{19}F NMR spectrum recorded at a temperature of 28 °C using a mixing time of 2 ms is shown in Figure 8a. Intense cross-correlation peaks between all the resonances corresponding to the F sites of the isolated $Al1F_6^{3-}$ octahedron (F2, F3, F4, and F5) are observed, revealing chemical exchange between these F ions on a time scale of 2 ms. In contrast, the 2D spectrum shows exclusively diagonal peaks for the nonbridging (F1) and bridging (F7 and F8) F atoms of the $Al2F_6^{3-}$ octahedra and for the free F ion (F6), indicating that they do not take part in the exchange process at least at T = 28 °C. The mutual exchange between all of the F ions of the isolated $Al1F_6^{3-}$ octahedral unit can be described as rotational discrete hops of the whole octahedron, as reported for AlF_6^{3-} octahedra in Na_3AlF_6[34] and for GaF_6^{3-} octahedra in $Pb_5Ga_3F_{19}$.[12] It should be noted that this motion does not lead to a significant averaging of the quadrupolar coupling interaction of the Al1 site in the temperature range 28−45 °C because the C_Q value calculated for a rigid structure (at T = 0 K) is very close to the experimentally measured C_Q value at T = 45 °C.

At a higher temperature of 90 °C, the MAS EXSY ^{19}F NMR spectrum recorded with the same mixing time of 2 ms (Figure 8b) exhibits cross-correlation peaks between line B (the motionally averaged signature of the four resonances of the $Al1F_6^{3-}$ unit) and both the F1 site and the free F ion F6, showing that they are now involved in a common chemical exchange. The bridging F ions F7 and F8 remain excluded from this process, which could also be related to longer F6−F7,8 distances (d_{F-F} > 5.6 Å; see the SI). This chemical exchange differs from the rotation of the $Al1F_6^{3-}$ octahedra and should involve the breaking and rebuilding of chemical bonds. This dynamical process is not revealed on the MAS ^{19}F NMR spectrum recorded at 90.5 °C because it occurs at a rate smaller than the frequency differences $\Delta\nu$ of these resonances (i.e., $\tau_c > 4 \times 10^{-4}$ s).

A complementary insight about the mobility of F atoms in the structure can be obtained by making use of the F−F homonuclear dipolar interaction, which was avoided or minimized in the EXSY experiments. In the presence of dynamical processes, the static dipolar interaction, which is directly related to interatomic spatial proximities, can be partly or fully averaged depending on the type and on the time scale of the atomic and molecular motions. Therefore, 2D homonuclear dipolar double-quantum

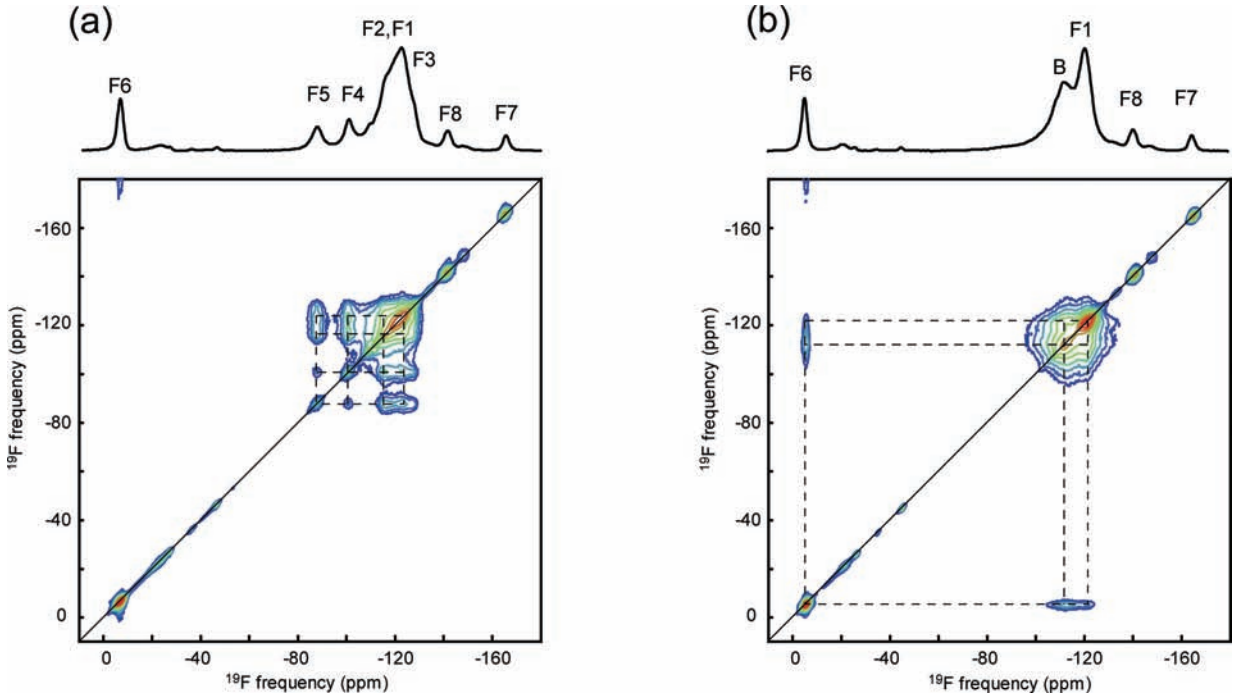

Figure 8. MAS EXSY ^{19}F NMR (54 kHz) spectra of $Ba_5Al_3F_{19}$ recorded with a mixing time of 2 ms at (a) T = 28 °C and (b) T = 90 °C. The thick line indicates the diagonal of the 2D spectrum. The dashed lines indicate cross-correlation peaks. The 1D MAS ^{19}F NMR spectra recorded at 28 and 90 °C are shown on top of the 2D maps with the line assignment based on the ^{19}F isotropic chemical shift DFT calculations for the geometry-optimized structure.

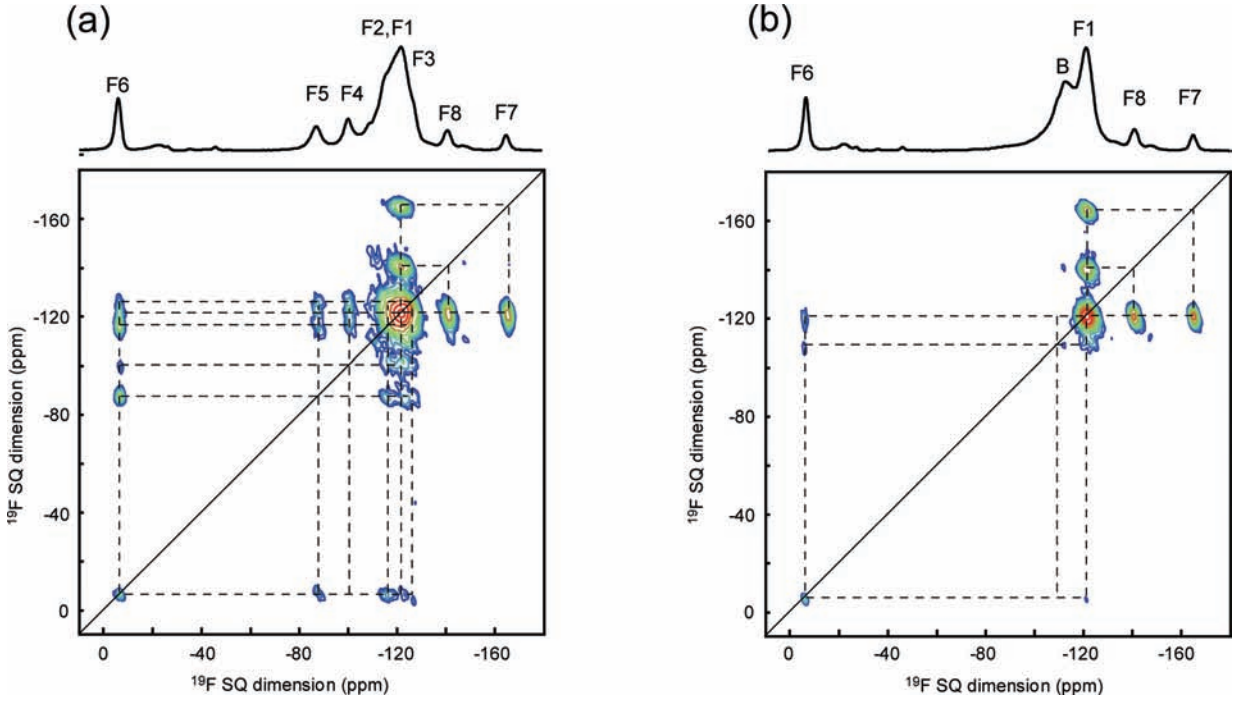

Figure 9. Sheared experimental 2D DQ−SQ MAS ^{19}F NMR (54 kHz) correlation spectra of $Ba_5Al_3F_{19}$ recorded at (a) T = 28 °C and (b) T = 90 °C. The thick lines indicate the diagonal of the 2D spectrum on which autocorrelation peaks appear. Cross-correlation peaks are indicated by the dashed lines. The 1D MAS ^{19}F NMR spectra recorded at 28 and 90 °C are shown on top of the 2D maps, with the line assignment based on the ^{19}F isotropic chemical shift DFT calculations for the geometry-optimized structure.

single-quantum (DQ−SQ) MAS correlation spectra were also recorded at T = 28 and 90 °C using the broad-band DQ dipolar recoupling SPIP[23] sequence with DQ excitation and reconversion times of 222 μs. These experiments were performed at a spinning frequency of 54 kHz using a moderate magnetic field of 7.0 T, for which the ^{19}F NMR spectrum of

dx.doi.org/10.1021/ic102534d |*Inorg. Chem.* 2011, 50, 2644–2653

$Ba_5Al_3F_{19}$ extends over ~48 kHz. This allows rotor synchronization of the indirect DQ dimension (which is necessary to avoid rotor-encoded DQ spinning side-band patterns[45−47] when using the SPIP recoupling sequence) without folding the 2D correlation spectrum in a SQ−SQ representation. In the obtained 2D spectrum, spatial proximities between inequivalent F sites are revealed by off-diagonal cross-correlation diagonal peaks, while proximities between equivalent F sites give rise to diagonal autocorrelation peaks. The sheared 2D homonuclear DQ−SQ MAS correlation spectrum recorded at $T = 28$ °C, i.e., in the slow dynamic regime ($\tau_c > 2\pi D^{-1}$, where D is the dipolar coupling constant), is shown in Figure 9a. As expected,[24,45,48] it exhibits intense correlation peaks between the individual resonances of each AlF_6^{3-} octahedral unit, which correspond to the shortest F−F interatomic distances (strongest F−F dipolar couplings) and correlation peaks of weaker intensities revealing longer range F−F dipolar interactions between the F sites of the $Al1F_6^{3-}$ and $Al2F_6^{3-}$ units (see Table S2 in the SI). Similar trends are also observed for the correlation peaks of the free F6 ion. The sheared 2D DQ−SQ ^{19}F NMR correlation spectrum recorded at 90 °C is shown in Figure 9b. At this temperature, the F sites of the isolated $Al1F_6^{3-}$ octahedron are in a fast dynamic regime ($\tau_c \ll 2\pi D^{-1}$) and the intramolecular F−F dipolar couplings are averaged to zero by the rotational motion of the whole octahedron, as evidenced by the absence of an autocorrelation peak for the resonance B in the 2D spectrum. In contrast, the chemical exchange between the F atoms of the $Al1F_6^{3-}$ octahedra and both the free F ion F6 and the nonbridging F atom of the $Al2F_6^{3-}$ octahedra (F1; evidenced from the EXSY MAS experiment) occurs at a slow time scale with respect to the strength of the corresponding dipolar couplings, giving rise to off-diagonal peaks located at the frequencies of the F6 and F1 resonances in the direct dimension and the frequency of line B in the indirect dimension on the 2D spectrum. Similarly, observation of an intense F1−F1 autocorrelation and F1−F7 and F1−F8 cross-correlation peaks (with intensities similar to those of the 2D spectrum recorded at 28 °C) indicates that the chains of $Al2F_6^{3-}$ octahedra remain rigid with respect to the dipolar couplings time scale and the presence of the F6−F6 autocorrelation peak shows that the fast hopping motion of the F6 ion between crystallographically equivalent sites can be excluded.

CONCLUSION

The room temperature structure of $Ba_5Al_3F_{19}$, solved by combining data from electron microscopy, SPD, MAS ^{27}Al and ^{19}F NMR experiments, is isostructural to that of $Pb_5Al_3F_{19}$-II. The ^{19}F isotropic chemical shift and ^{27}Al quadrupolar parameters of $Ba_5Al_3F_{19}$ have been calculated using the *CASTEP* code for the experimental and DFT geometry-optimized structures. The NMR parameters of both the ^{19}F and ^{27}Al nuclei calculated for the geometry-optimized structure show a better consistency with the experimental ones, indicating that the geometry optimization step is necessary to obtain more accurate and reliable structural data. These calculations also allow a complete and unambiguous assignment of the ^{19}F NMR resonances to the distinct crystallographic F sites of the $Ba_5Al_3F_{19}$ structure. VT 1D MAS ^{19}F NMR experiments have been carried out, showing the occurrence of fluorine ion mobility. Complementary insights were obtained from both 2D exchange and double-quantum dipolar recoupling NMR experiments. Two distinct types of fluorine anionic motion occurring with distinct correlation times are evidenced in $Ba_5Al_3F_{19}$: a fast reorientation of the $Al1F_6^{3-}$ octahedra and a slower chemical exchange involving bond breaking and re-formation. The current study of $Ba_5Al_3F_{19}$ clearly illustrates that the combination of X-rays and electron powder diffraction with VT high-resolution solid-state NMR experiments and DFT calculation of the NMR parameters allows one to obtain accurate and reliable structural data and also can contribute to a detailed analysis of anionic motion.

ASSOCIATED CONTENT

Supporting Information. CIF files of the SPD and DFT geometry-optimized structures of $Ba_5Al_3F_{19}$, Ba−F and F−F interatomic distances (SPD and geometry-optimized structures), and diffraction diagram calculated from the DFT geometry-optimized structure of $Ba_5Al_3F_{19}$. This material is available free of charge via the Internet at http://pubs.acs.org.

AUTHOR INFORMATION

Corresponding Author

*E-mail: charlotte.martineau@chimie.uvsq.fr. Tel: +33139254260. Fax: +33139254476.

ACKNOWLEDGMENT

C.M. and F.T. are grateful to Prof. A. de Kozak for providing the sample. The use of the Advanced Photon Source at Argonne National Laboratory was supported by the U.S. Department of Energy, Office of Science, Office of Basic Energy Sciences, under Contract DE-AC02-06CH11357.

REFERENCES

(1) de Kozak, A.; Samoüel, M.; Renaudin, J.; Férey, G. *Z. Anorg. Allg. Chem.* **1992**, *613*, 98–104.
(2) Domesle, R.; Hoppe, R. *Angew. Chem., Int. Ed.* **1980**, *19*, 489–490.
(3) Kaizer, V.; Babel, D. *Z. Anorg. Allg. Chem.* **2004**, *630*, 794–798.
(4) Abrahams, S. C.; Marsh, P.; Ravez, J. *J. Chem. Phys.* **1987**, *87*, 6012–6020.
(5) Graulich, J.; Babel, D. *Z. Anorg. Allg. Chem.* **1991**, *597*, 51–59.
(6) Dahlke, P.; Graulich, J.; Welsh, M.; Pebler, J.; Babel, D. *Z. Anorg. Allg. Chem.* **2000**, *626*, 1255–1263.
(7) Abrahams, S. C.; Albertsson, J.; Svensson, C.; Ravez, J. *Acta Crystallogr.* **1990**, *B46*, 467–502.
(8) Sarraute, S.; Ravez, J. *Acta Crystallogr.* **1995**, *C51*, 1731–1732.
(9) Sarraute, S.; Ravez, J.; Von Der Mühll, R.; Bravic, G.; Feigelson, R. S.; Abrahams, S. C. *Acta Crystallogr.* **1996**, *B52*, 72–77.
(10) Martineau, C.; Fayon, F.; Legein, C.; Buzaré, J.-Y.; Goutenoire, F.; Suard, E. *Inorg. Chem.* **2008**, *47*, 10895–10905.
(11) Welsh, M.; Holler, H.; Babel, D. *Z. Anorg. Allg. Chem.* **1989**, *575*, 171–186.
(12) Martineau, C.; Fayon, F.; Legein, C.; Buzaré, J.-Y.; Corbel, G. *Chem. Mater.* **2010**, *22*, 1585–1594.
(13) Body, M.; Silly, G.; Legein, C.; Buzaré, J.-Y.; Calvayrac, F.; Blaha, P. *J. Solid State Chem.* **2005**, *178*, 3655–3661.
(14) Martineau, C.; Fayon, F.; Legein, C.; Buzaré, J.-Y.; Body, M.; Massiot, D.; Goutenoire, F. *Dalton Trans.* **2008**, 6150–6158.
(15) Segall, M. D.; Lindan, P. L. D.; Probert, M. J.; Pickard, C. J.; Hasnip, P. J.; Clark, S. J.; Payne, M. C. *J. Phys.: Condens. Matter* **2002**, *14*, 2717–2744.
(16) Clark, S. J.; Segall, M. D.; Pickard, C. J.; Hasnip, P. J.; Probert, M. J.; Refson, K.; Payne, M. C. *Z. Kristallogr.* **2005**, *220*, 567–570.

(17) Rietveld, H. M. *J. Appl. Crystallogr.* **1969**, *2*, 65–71.
(18) Carjaval, J. R. *FULLPROF Program, Rietveld Pattern Matching Analysis of Powder Patterns*; ILL: Grenoble, France, 1990.
(19) Van Gorkom, L. C. M.; Hook, J. M.; Logan, M. B.; Hanna, J. V.; Wasylishen, R. E. *Magn. Reson. Chem.* **1995**, *33*, 791–795.
(20) Bielecki, A.; Burum, D. P. *J. Magn. Reson., Ser. A* **1995**, *116*, 215–220.
(21) Szeverenyi, N. M.; Bax, A.; Maciel, G. E. *J. Am. Chem. Soc.* **1983**, *105*, 2579–2582.
(22) States, D.; Haberkorn, R.; Ruben, D. *J. Magn. Reson.* **1982**, *48*, 286–292.
(23) Hu, B.; Wang, Q.; Lafon, O.; Trébosc, J.; Deng, F.; Amoureux, J. P. *J. Magn. Reson.* **2009**, *198*, 41–48.
(24) Wang, Q.; Hu, B.; Fayon, F.; Trébosc, J.; Legein, C.; Lafon, O.; Deng, F.; Amoureux, J. P. *Phys. Chem. Chem. Phys.* **2009**, *11*, 10391–10395.
(25) Wang, Q.; Hu, B.; Lafon, O.; Trébosc, J.; Deng, F.; Amoureux, J. P. *J. Magn. Reson.* **2010**, *203*, 113–138.
(26) Ernst, R. R.; Bodenhausen, G.; Wokaun, A. *Principles of Nuclear Magnetic Resonance in One and Two Dimensions*; Clarendon Press: Oxford, U.K., 1987.
(27) Fayon, F.; King, I. J.; Harris, R. K.; Gover, R. K. B.; Evans, J. S. O.; Massiot, D. *Chem. Mater.* **2003**, *15*, 2234–2239.
(28) Massiot, D.; Fayon, F.; Capron, M.; King, I.; Le Calvé, S.; Alonso, B.; Durand, J. O.; Bujoli, B.; Gan, Z.; Hoatson, G. *Magn. Reson. Chem.* **2002**, *40*, 70–76.
(29) Profeta, M.; Mauri, F.; Pickard, C. J. *J. Am. Chem. Soc.* **2003**, *125*, 541–548.
(30) Pickard, C. J.; Mauri, F. *Phys. Rev. B* **2001**, *63*, 245101.
(31) Perdew, J. P.; Burke, K.; Ernzerhof, M. *Phys. Rev. Lett.* **1996**, *77*, 3865–3868.
(32) Yates, J. R.; Pickard, C. J.; Mauri, F. *Phys. Rev. B* **2007**, *76*, 024401.
(33) Pfrommer, B. G.; Cote, M.; Louie, S. G.; Cohen, M. L. *J. Comput. Phys.* **1997**, *131*, 233–240.
(34) Du, L.-S.; Levitt, M. H.; Grey, C. P. *J. Magn. Reson.* **1999**, *140*, 242–249.
(35) Body, M.; Legein, C.; Buzaré, J.-Y.; Silly, G. *Eur. J. Inorg. Chem.* **2007**, *14*, 1980–1988.
(36) Body, M.; Legein, C.; Buzaré, J.-Y.; Silly, G.; Blaha, P.; Martineau, C.; Calvayrac, F. *J. Phys. Chem. A* **2007**, *111*, 11873–11884.
(37) Body, M.; Silly, G.; Legein, C.; Buzaré, J.-Y. *Inorg. Chem.* **2004**, *43*, 2474–2485.
(38) Bureau, B.; Silly, G.; Emery, J.; Buzaré, J.-Y. *Chem. Phys.* **1999**, *249*, 89–104.
(39) Zheng, A.; Liu, S. B.; Deng, F. *J. Phys. Chem. C* **2009**, *113*, 15018–15023.
(40) Ghose, S.; Tsang, T. *Am. Mineral.* **1973**, *58*, 748–755.
(41) Suter, D.; Ernst, R. R. *Phys. Rev. B* **1985**, *32*, 5608–5627.
(42) Henrichs, P. M.; Linder, M.; Hewitt, J. M. *J. Chem. Phys.* **1986**, *85*, 7077–7086.
(43) Kubo, A.; McDowell, C. A. *J. Chem. Phys.* **1988**, *89*, 63–70.
(44) Reichert, D.; Bonagamba, T. J.; Schmidt-Rohr, K. *J. Magn. Reson.* **2001**, *151*, 129–135.
(45) Brown, S. P. *Prog. Nucl. Magn. Reson. Spectrosc.* **2007**, *50*, 199–251.
(46) Graf, R.; Demco, D. E.; Gottwald, J.; Hafner, S.; Spiess, H. W. *J. Chem. Phys.* **1997**, *106*, 885–895.
(47) Friedrich, U.; Schnell, I.; Brown, S. P.; Lupulescu, A.; Demco, D. E.; Spiess, H. W. *Mol. Phys.* **1998**, *95*, 1209–1227.
(48) Martineau, C.; Legein, C.; Buzaré, J.-Y.; Fayon, F. *Phys. Chem. Chem. Phys.* **2009**, *11*, 950–957.